

ARTICLE OPEN



MS4A4A promotes macrophages M2 polarization via NF- κ B /JAK-STAT6 axis, resulting GBM malignant progression

Ziwei Li^{1,11}, Wu Chunfa^{2,11}, Zhongliang Cui^{1,11}, Bo Liang^{3,4}, Chen Wang¹, Mingchen Yu⁵, Yishuo Sun¹, Di Wang¹, You Zhai^{1,5}, Changqing Pan¹, Jiazheng Zhang¹, Zhongfang Shi⁶, Tao Jiang^{1,5,7,8,9} and Wei Zhang^{1,5,7,8,9,10}

© The Author(s) 2026

The immunosuppressive tumor microenvironment (TME) is a major issue in the malignant progression of glioma patients. The membrane spanning four domains A4A (MS4A4A) has a relationship with M2 polarization of macrophages, and participates in the malignant progression of various cancers. Therefore, exploration of the key role of MS4A4A contributing to glioma biological processes is urgently needed. We performed the bioinformatics analysis of M2 gene expression and built a model predicting the prognosis of glioma patients. Knocking down or overexpressing MS4A4A was achieved in macrophages, and we identified the polarization of macrophages with different MS4A4A expression levels. In vitro and in vivo experiments were used to investigate the role of MS4A4A in regulating M2 polarization and contributing to malignant behaviour in glioma. We found that MS4A4A was associated with the macrophages' M2 scores and the prognosis of GBM patients. MS4A4A had a higher expression level in M2 polarization macrophages. MS4A4A regulates macrophage M2 polarisation through NF- κ B and JAK-STAT6 signalling pathways. Macrophages with MS4A4A overexpression promoted the proliferation, invasion, and TMZ-resistance of glioma cells in vitro and in vivo experiments. The treatment targeting the MS4A4A/ NF- κ B/STAT6 axis could improve the prognosis and TMZ-resistance in the glioma mouse model. The present study revealed the novel mechanism of the MS4A4A regulating macrophages M2 polarization, contributing to the formation of immunosuppressive tumor microenvironment in glioma through NF- κ B/STAT6 signaling pathways, which promotes the malignant biological process of glioma cells. Our results provided new evidence that NF- κ B and STAT6 inhibitors might be a potential adjuvant agent in overcoming MS4A4A-mediated chemotherapy resistance in glioma.

Oncogene; <https://doi.org/10.1038/s41388-026-03773-1>

INTRODUCTION

Glioma is the most common malignant brain tumor of the central nervous system in adults [1]. Although taking the aggressive comprehensive treatment, the median overall survival of glioblastoma (GBM) patients only remains to be approximately 12 to 14 months [2]. The formation of an immunosuppressive tumor microenvironment plays an important role in malignant biological behavior of GBM [3]. Similar to other tumors, macrophages are one of the major components of GBM microenvironment [4], and the polarization regulates the extracellular matrix remodeling, cancer cell proliferation, metastasis and immunosuppression, as well as resistance to chemotherapeutic agents [5]. Our previous study illustrated that the cross-talk between GBM cells and microglia could remodel the microenvironment and reduce tumor sensitivity to TMZ chemotherapy [6]. Therefore, deepening the underlying mechanism regulating immunosuppressive microenvironment may improve the therapy strategy of GBM patients.

The membrane spanning four domains A4A (MS4A4A) is one member of the membrane-spanning 4A family, including 18 members with a tetraspan structure in humans [7]. MS4A4A has selective expression in macrophages and is co-expressed with M2/ M2-like molecules in subsets of normal tissue-resident macrophages, infiltrating macrophages from inflamed synovium and tumor-associated macrophages [8]. In colorectal cancer, the blockade of MS4A4A could reshape the tumor immune microenvironment, increasing the infiltration of effector CD8 T cells, and enhancing the efficacy of immune checkpoint inhibitors [9]. However, the underlying mechanism of MS4A4A regulating the GBM immune microenvironment needs to be further investigated.

The nuclear factor- κ B (NF- κ B) could be activated by canonical and non-canonical pathways, differing in both signaling components and biological functions [10]. It has been shown that NF- κ B serves as a molecular lynchpin, linking persistent infections and chronic inflammation to increased cancer risk [11]. In our previous

¹Department of Neurosurgery, Beijing Tiantan Hospital, Capital Medical University, Beijing, PR China. ²Department of Neurosurgery, The First Hospital of Shanxi Medical University, Taiyuan, PR China. ³Beijing Neurosurgical Institute, Capital Medical University, Beijing, PR China. ⁴Department of Neurosurgery, Beijing Ditan Hospital, Capital Medical University, Beijing, PR China. ⁵Department of Molecular Neuropathology, Beijing Neurosurgical Institute, Capital Medical University, Beijing, PR China. ⁶Department of pathophysiology, Beijing Neurosurgical Institute, Beijing Tiantan Hospital, Beijing, PR China. ⁷China National Clinical Research Center for Neurological Diseases, Beijing, PR China. ⁸Beijing Engineering Research Center of Targeted Drugs and Cell Therapy for CNS Tumors, Beijing, PR China. ⁹Chinese Glioma Genome Atlas Network (CGGA) and Asian Glioma Genome Atlas Network (AGGA), Beijing, PR China. ¹⁰Brain Tumor Center, Beijing Institute of Brain Disorders, Capital Medical University, Beijing, PR China. ¹¹These authors contributed equally: Ziwei Li, Chunfa Wu, Zhongliang Cui. ✉email: shizhongfangbj@163.com; taojiang1964@163.com; zhangwei_vincent@mail.ccmu.edu.cn

Received: 10 May 2025 Revised: 11 March 2026 Accepted: 30 March 2026

Published online: 29 April 2026

study, we found that NF- κ B-related LINC001127, regulated by the histone lactylation induced by the Warburg effect, could promote the renewal of GBM cells [12]. Recent studies have revealed that the NF- κ B pathway plays an important role in regulating different aspects of immune function during the progression of various cancers, which may provide new opportunities for therapeutic strategies [13, 14]. The specific silencing of NF- κ B signaling could inhibit the tumor-associated macrophages (TAMs)-driven cancer progression [15]. In this study, we deepened the role of NF- κ B in remodeling the GBM immune microenvironment regulated by MS4A4A and tried to find a novel combined therapeutic strategy to improve the TMZ treatment efficacy.

JAK-STAT6 signaling pathway has crucial functions in regulating biological processes in many cell types of organisms, used to be considered the key dysregulating pathway in chronic inflammatory disease, atherosclerosis, and blood system diseases [16–18]. Recently, many studies demonstrated that the JAK-STAT6 pathway and its target genes participated in the progression of lung cancer and lymphoma [19, 20]. In gliomas, the activity of the JAK-STAT6 pathway may regulate the proliferation, metabolic reprogramming, DNA repair, and epithelial-mesenchymal transition (EMT) [21]. The researchers have newly focused on the effect of the JAK-STAT6 pathway regulating macrophage differentiation and remodeling the tumour microenvironment [22, 23]. Thus, we proposed that the JAK-STAT6 pathway might be implicated in the M2 polarization of macrophages, regulating the GBM microenvironment remodeling.

In the present study, we investigated the role of MS4A4A in regulating TAMs M2 polarization and the malignant biological progression of GBM cells. Our results indicated that MS4A4A was associated with higher M2 scores and poorer prognosis of GBM patients. MS4A4A regulated M2 polarization of macrophages via NF- κ B/STAT6 signaling pathways, and the GBM immunosuppressive microenvironment remodeling promoted the proliferation, invasion, and TMZ-resistance of GBM cells. The combined inhibitors together enhanced TMZ treatment efficiency in GBM organoid and xenograft models, indicating that NF- κ B/STAT6 inhibitors might be a potential adjuvant agent in overcoming MS4A4A-mediated malignant behavior in GBM.

METHODS

Data collection

The RNA sequencing (RNA-seq) data of normal tissues were obtained from the Genotype-Tissue Expression Project (GTEx) database (<https://www.gtexportal.org>). The glioma RNA-seq data (TCGA_mRNAseq_709, a total of 704 cases, including GBM and LGG) and clinical information were obtained from the TCGA website (<http://portal.gdc.cancer.gov>). The TCGA database includes clinical data such as gender, age, WHO malignancy grades, survival time, and survival status. The mRNAseq [24, 25] was downloaded from the China Glioma Genome Atlas database (CGGA, mRNAseq_693). CGGA database (<http://www.cgga.org.cn/download.jsp>) contains detailed clinical data, such as gender, age, IDH status, 1p19q co-deletion status, MGMT status, radiotherapy and chemotherapy, complete follow-up data, WHO malignancy grades, and primary-recurrence status [26].

Macrophages M2-related genes analysis

The CIBERSORT algorithm in R 4.3.0 was used to obtain the relative immune infiltration levels of 22 immune cell types for each sample in the TCGA database. The genes in GBM samples co-expressing with M2 macrophages were identified and defined as M2-related genes (Spearman ≥ 0.6 , $P < 0.001$) by co-expression analysis. The igraph package was used to visualize the network diagram of M2-related genes.

Model building and validation

The cross of M2-related genes was selected in the TCGA and CGGA databases, and the expression level of M2-related genes was calculated for each database. The expression data of M2-related genes were further

combined with survival information (survival time and survival status) of GBM samples. The M2-related genes associated with prognosis were analyzed in the TCGA database ($P < 0.05$) using survival and survminer R packages. The least absolute shrinkage and selection operator (LASSO) regression model was constructed using the TCGA database as the training set, utilizing the lambda and survival packages. The x-axis represented gene expression, and the y-axis represented survival time. Cross-validation was used to find the point with the minimum cross-validation error, resulting in the model formula. Based on the formula, the risk score for each sample was calculated. Using the median risk score, GBM samples from both the TCGA and CGGA databases were divided into high- and low-risk groups.

To validate the accuracy of the prognostic model, the CGGA database was used as a test group, and the difference in survival time between high-risk and low-risk groups of GBM patients was identified by the survival and survminer R packages. The timeROC package was used to construct receiver-operating characteristic (ROC) curves and calculate the area under the curve (AUC) values at 1, 3, and 5 years to assess the predictive value of prognostic survival models.

Cell culture

The human glioma cell line LN229, mouse glioma cell line GL261, human macrophage cell line THP-1, and mouse macrophage cell line Raw264.7 were purchased from the Chinese Academy of Sciences Cell Bank. The STR assay was used to authenticate these cells. All the cell lines used in this study were cultured in RPMI-1640, Dulbecco's modified Eagle's medium (DMEM), DMEM/F12 (Corning, USA) supplemented with 10% fetal bovine serum (FBS; BD Biosciences, USA) and 1% antibiotic solution (Sigma, Germany) at 37 °C in a humidified atmosphere with 5% CO₂ and 95% air. All cells were starved in 2% serum medium for 12 h before being treated with conditioned medium or different drugs.

Western blot assay

Prechilled RIPA buffer (Solarbio, China) combined with 1% proteinase and phosphatase inhibitor cocktails (Selleck, USA) was used to extract the total protein from different treating cells. Subsequently, the protein samples were subjected to 7.5%/10%/12.5% sodium dodecyl sulfate polyacrylamide gel (EpiZyme Scientific) electrophoresis in a volume of 10 to 20 μ L. The 5% BSA-TBST solution was used to block PVDF membranes. The PVDF membranes were then incubated overnight at 4 °C with primary antibodies (Supplementary Table S1). HRP-labeled mouse IgG secondary antibodies (Zsbio Store-bio, China) and HRP-labeled rabbit IgG secondary antibodies (Zsbio Store-bio, China) were used to incubate the membranes. The chemiluminescence reagent (ECL) kit (Boster, USA) was used to visualize the protein bands. Protein quantification was analyzed by Image Lab.

Single-cell sequencing

The GBM sample single-cell RNA libraries were established following the STRT-seq protocol in our previous studies [27, 28]. The Illumina platform (HiSeq 4000) was used to sequence the libraries according to the manufacturer's instructions by Novogene (Beijing, China).

Cell transfection

The MS4A4A and Ms4a4a small-interference RNA (siRNA) and negative control were purchased from RiboBio Co., Ltd (Guangzhou, China). The transfection reagent (Polyplus-transfection Co., Ltd., France) was used to transfect the macrophages with siRNA or negative control 50 nM at 37 °C. After 48 h of incubation, the cells were cultured with fresh medium without siRNA. The sequences of siRNA and negative control used in this study are shown in Supplementary Table S2.

MS4A4A/Ms4a4a overexpressing lentivirus and the scramble control were synthesized by and purchased from Syngenebio Company (Shanghai, China). THP-1 and Raw264.7 cells were infected with MS4A4A/Ms4a4a overexpressing lentivirus according to the manufacturer's instructions. The vectors in this study were pLV-hef1a-Puro-WPRE-CMV-MCS-3flag.

Hematoxylin-eosin staining and immunohistochemical

For H&E staining, the mouse GBM slides under deparaffinization and rehydration were stained in hematoxylin solution (Zsbio Store-bio, China) for 8 min and in eosin-phloxine solution (Zsbio Store-bio, China) for 30 seconds to 1 min, then mounted with xylene.

For IHC staining, briefly, paraffin-embedded GBM tissue sections were incubated at 80 °C for 15 min, dewaxed in xylene, washed in gradient ethanol solutions, and rehydrated in double-distilled water. Then, the slides were pretreated by steaming them in sodium citrate buffer for 15 min at 95 °C to restoring antigen. After washing 3 times for 5 min, the slides were incubated with the indicated primary antibodies (Supplementary Table S1) at 4 °C overnight. The HRP-labeled either anti-mouse IgG or anti-rabbit IgG (Zsbio Store-bio, China) secondary were used to incubate the slides for 30 min. DAB staining kit (Zsbio Store-bio, China) was used to dye the GBM tissue slides for 2 min. Quantitative evaluation was performed by examining each section using at least 10 different high-power fields with the most abundant stained cells. The intensity was graded depending on the number of positive cells seen: “-” no staining, “+” weak staining, “++” moderate staining, and “+++” intense staining.

Immunofluorescence

Cells were placed on the cell coverslips (WHB-24-CS, China) in 24-well tissue culture plates overnight. After incubation in 4% formaldehyde for 15 min at room temperature, the cells were rinsed three times in PBS for 5 min. Then we treated the cells with 0.3% Triton-X100 (Thermo Fisher, USA) and blocked them in 5% BSA-PBS blocking buffer (BioFroxx, Germany) for 60 min in room temperature. The diluted primary antibodies (Supplementary Table S1) were added and incubated at 4 °C overnight. After washing 3 times with PBS, the cells were incubated with FITC-labeled anti-IgG antibodies (Alexa Fluor 488 and 594, Thermo Fisher, USA) for 1 hour at room temperature. DAPI (Sigma, USA) was applied to dye the DNA. The subcellular location of the indicated proteins was visualised with a fluorescence microscope (Nikon C2).

RNA isolation, polymerase chain reaction, and quantitative real-time polymerase chain reaction

TRIzol reagent (Invitrogen, USA) was used to extract the total RNA according to the manufacturer's instructions. cDNAs were synthesized with the PrimeScript RT reagent Kit (TaKaRa, Japan). In the final reaction volume of 20 µL, 2 µL cDNA was used at a concentration of 100 ng/mL. Triplicate samples in a reaction mix (TaKaRa, Japan) were subjected to real-time quantitative polymerase chain reaction (PCR). CFX96 Touch Real-Time PCR Detection System (Bio-Rad) was applied to conduct the PCR and qRT-PCR assays, and the indicated genes were normalized to β-actin. The qRT-PCR data were analyzed using the $2^{-\Delta\Delta Ct}$ method. The primer design tool (<http://www.ncbi.nlm.nih.gov/tools/primer-blast/>) was used to design and synthesized the PCR primers. The primer sequences used in this study are listed in Supplementary Table S3.

Flow cytometry

For flow cytometry assays, FITC anti-Human/Mouse Arg-1 (Bio-Techne, USA) were used for the M2 polarization macrophage surface marker determination. The cells were washed in PBS containing 2% BSA (BioFroxx, Germany) for 1 hour with the indicated antibodies. The expression of macrophages surface markers was determined by flow cytometry using BD Accuri C6 and analyzed by FlowJo.

To detect the rates of different treated GBM apoptosis, Annexin V-FITC Apoptosis Detection Kit (BD Biosciences, USA) was applied according to the manufacturer's instructions. Then, the rates of apoptosis were measured by flow cytometry through BD Accuri C6 and analyzed by FlowJo.

CCK-8 assay, transwell assay and cell scratch assay

For the CCK-8 assay, the Cell Counting Kit 8 (CCK-8, Dojindo, Japan) was applied based on the manufacturer's instructions to evaluate the viability of different cells. The BioTek Gen5 system (BioTek) was used to measure the OD 450 nm of cell viability.

In Transwell assays, different treated GBM cells were seeded into upper chambers of the 24-well Transwell chambers (Corning, USA) in a 200 µL serum-free culture system, while 600 µL medium containing 10% FBS was added into the lower chamber. After the incubation at 37 °C for 2 to 4 h, the cells on the upper surface of the filters were removed with cotton swabs and the cells at the bottom surface were fixed and dyed by 0.5% crystal violet.

For cell scratch assays, GBM cells with different treatments were placed in 6-well plates with 1×10^5 cells per well and cultured at 37 °C for adherence. Then, a sterile 200-µL pipette tip was used to scrape the cell monolayer in every well. The culture medium was replaced with the medium without serum, and the “zero point” of migration in each well was obtained under computer-assisted microscopy (ZEISS, Germany). At the

endpoint of 48 h incubation, the corresponding scratch area of each well was photographed again.

Comet assay

The cells with different treatments were seeded, resuspended in 100 µL of 10% low-melting-point agarose (Promega, USA), and placed on a microscope slide and gelled at 4 °C for 20 min. Subsequently, the cells were immersed in the cell lysis solution (Trevigen, USA) and lysed at 4 °C for 1 to 2 h according to the manufacturer's instructions. Then the slides were washed in distilled water and electrophoresed in electrophoresis solution (Y-J Biological, China) with an electric field (25 V, 300 mA) for 30 min. After neutralized, the SYBR Green (Sangon, China) was used to stain the slides. Tail length and percentage of DNA in tail, indicating the level of DNA damage, were analyzed by ImageJ.

Establishment of GBM organoid

NanoShuttleTM-PL (Greiner Bio-One) with the concentration of 1 µL NanoShuttles/10000 cells was used to incubate the GBM patients-derived single cell suspensions. Then, the cells were placed in a 96-well plate (WHB-24-CS, China) at a density of 50000 cells per well in 150-200 µL culture medium. To aggregate the cells to the well bottom, we placed the 96-well plate on the top of a spheroid drive for 15 min at 37 °C. DMEM/F-12 medium with BIT supplement (Thermo Fisher, USA), bFGF (Thermo Fisher, USA) and EGF (Thermo Fisher, USA) was applied to culture GBM organoid for 5 days. The cell viability of GBM organoids was detected by LIVE/DEAD Cell Imaging Kit (Invitrogen) according to the manufacturer's instructions.

Drug treatment

DMSO (Selleck, USA) was used to dissolve the temozolomide (TMZ, Selleck, USA), and the TMZ stock solution was stored at -80 °C for further experiments. Phorbol 12-myristate 13-acetate (PMA, Sigma-Aldrich, USA) with 100 ng/mL was used to incubate the macrophages for 24 h to induce their differentiation in vitro. IL-4 and IL-13 were purchased from Merck KGaA (Darmstadt, Germany) and used to induce macrophages M2 polarization with 20 ng/mL for 48 h. TMZ (Selleck, USA) was injected in vivo via intraperitoneal injection with 60 mg/kg. BAY 11-7082 (MedChemExpress, USA) and AS1517499 (MedChemExpress, USA) were used in the xenograft model in vivo at the doses of 15 mg/kg and 10 mg/kg via intraperitoneal injection.

Xenograft model in vivo

GBM xenografts were established with 4 to 6-week-old male C57BL/6 mice purchased from Beijing Vitalstar Biotechnology Co., Ltd (Beijing, China). Then, the GL261 cells transfected with luciferase lentivirus ($0.5-1 \times 10^6$ cells per mouse) mixed with macrophages with different Ms4a4a expression levels (0.2×10^6 cells per mouse) were stereotactically injected into the brain. After the implant of the GBM model for 7 days, mice were randomly separated into four groups, which were treated with DMSO, TMZ alone, or TMZ combined with the inhibitors every 2 days at the indicated doses. At days 7th, 14th, and 21st, the intracranial tumours were measured with bioluminescence imaging via intraperitoneal injection of D-Luciferin, Potassium Salt (Yeason, China) at a concentration of 150 mg/kg using an IVIS Lumina Imaging System (Xenogen). At the endpoint of in vivo experiments, the tissues of different groups of mice were extracted and fixed in 10% formalin for H&E and IHC staining.

Statistical analysis

The significant differences between different groups were assessed by the Student *t* test. The tumor growth curves were analyzed using two-way ANOVA, followed by Tukey's multiple comparison test via GraphPad software version 7.0. The survival distributions of different groups were described by overall survival curves, and the log-rank test was applied to assess statistical significance. Univariate and multivariate Cox regression analyses were performed to further process the survival data. Pearson's correlation coefficient was used to analyze the correlations between variables. Chi-squared test was used to estimate the comparisons between the quantitative evaluation of IHC assays. KEGG analysis was used with DAVID Bioinformatics (<https://david.ncifcrf.gov>), and differential expression analysis was performed by the GEPIA database (<http://gepia.cancer-pku.cn/>). All results are expressed as the mean ± SD. All statistical analyses were performed using GraphPad software version 7.0 (GraphPad Software). *P* < 0.05 was considered statistically significant.

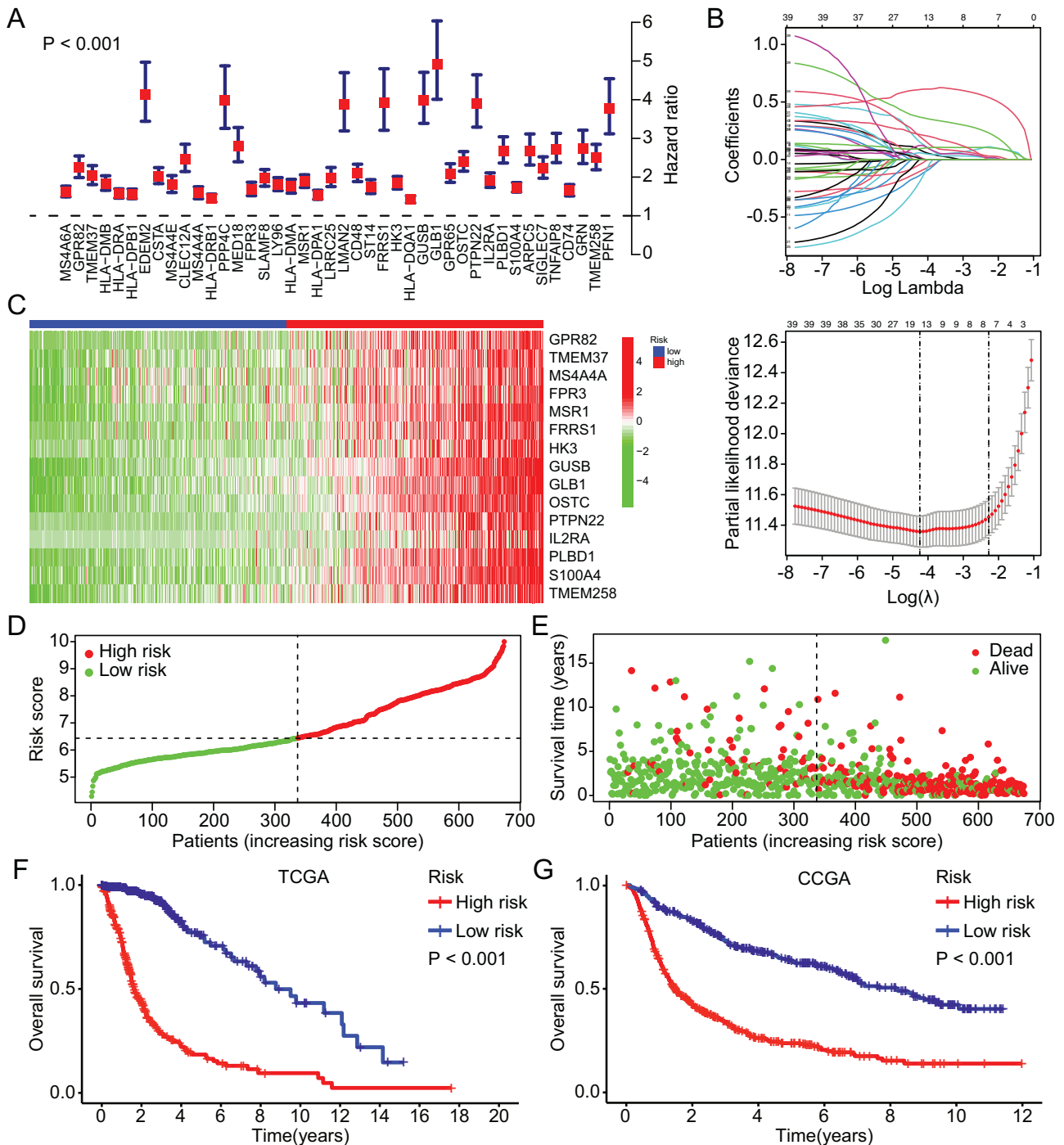


Fig. 1 MS4A4A is included in the LASSO regression model for the prognosis of GBM patients. **A** The related genes of macrophages M2 scores were shown in the forest plot. M2 scores were identified by CIBERSORT in TCGA database. **B** The establishment of LASSO regression model for the prognosis of GBM patients, the variation characteristics of the coefficient of variables and the selection process of the optimum value of the parameter λ in the LASSO regression model by cross-validation method. **C** The different expressing characteristics of high-risk and low-risk groups in TCGA database. **D** The risk scores for GBM samples in TCGA database. **E** The relationship between risk score and survival time of GBM samples in TCGA database. **F** The KM survival curves of the high- and low-risk groups in TCGA database. **G** The KM survival curves of the high- and low-risk groups in CCGA database.

RESULTS

The M2-related genes model predicts the prognosis of GBM patients

To investigate the influence of macrophages on GBM, we first screened the GBM samples for genes associated with macrophage M2 scores by calculating the relative content of 22 immune cells in the TCGA database and found 47 associated genes. All of 47

indicated genes were positive correlated with macrophages M2 scores shown in a network diagram (Supplementary Fig. 1A). Univariate Cox regression analysis was performed to identify 42 genes that were highly correlated and critical for poorer survival (Fig. 1A). Then we further optimized the prognostic genes by the LASSO regression model, and constructed prognostic models for 15 genes from the 42 survival-related M2 genes, obtained the

optimal cut-off values for TCGA database (Fig. 1B). For LASSO model validation, we categorized the GBM samples in TCGA and CGGA database into high- and low-risk group. The model genes had different expression between the high-risk and low-risk groups in the TCGA and CGGA database, and all the 15 model genes were elevated in the high-risk group (Fig. 1C and Supplementary Fig. 1B). The GBM samples in the TCGA and CGGA database were sorted according to the risk score, which increased from left to right. We found that longer survival time mainly consisted of low-risk patients, and poorer survival mainly consisted of high-risk patients (Fig. 1D, E and Supplementary Fig. 1C, D). Moreover, we performed KM analysis to evaluate the high-risk and low-risk groups in the TCGA database, the CGGA database as the test group. The results showed that the difference in survival time between patients in high-risk and low-risk groups was consistent in the TCGA and CGGA databases. The risk scores could predict the survival of GBM patients in TCGA and CGGA databases (Fig. 1F, G). Then, we performed univariate and multivariate Cox analyses in TCGA and CGGA databases (Supplementary Fig. 1E–H) and found that the prognostic models are an independent validation of GBM prognostic significance. To assess the accuracy of the LASSO model in predicting the GBM patient's survival, we performed ROC curve analyses on the 1-, 3-, and 5-year survival rates of the TCGA database samples and the CGGA database samples, and found that AUC values were 0.874, 0.912, and 0.868 for the TCGA database, and AUC values of 0.722, 0.753, and 0.755 for the CGGA database. The areas under the ROC curves were all greater than 0.7, indicating that the prognostic model can predict the survival of patients well (Supplementary Fig. 2A–B). Based on the results of the multivariate Cox proportional hazards model, we performed a nomogram to predict the 1-year, 3-year and 5-year overall survival time of GBM patients (Supplementary Fig. 2C–F). Notably, we noticed that MS4A4A was involved in the 15 genes of prognostic models, which were important in regulating macrophage M2 polarization in colon cancer [9]. However, the mechanism of MS4A4A in remodeling GBM microenvironment remains unclear.

MS4A4A is associated with poor prognosis and M2 polarization in GBM

For further illustrate the roles of MS4A4A in GBM, we performed a comparative analysis to detect the relationship between the MS4A4A expression and the distinct patterns of clinical and pathological characteristics in GTEx and TCGA datasets. MS4A4A was highly enriched in GBM samples compared to normal tissues (Fig. 2A). Moreover, higher-grade GBM had an elevated expression level of MS4A4A (Fig. 2B). We collected the GBM samples and normal tissues, and found that MS4A4A had a significantly higher expression level in GBM samples (Fig. 2C, D). Then, we demonstrated that IDH-wildtype and GBM without 1p/19q codeletion had a higher MS4A4A expression level (Supplementary Fig. 3A, B). The GBM without MGMT promoter methylation had high MS4A4A expression in the TCGA dataset; however, this difference was not statistically significant in the CGGA dataset (Supplementary Fig. 3C).

In addition, we explored the expression level of MS4A4A in the four transcriptional subtyping defined by the TCGA datasets [29] and found that MS4A4A was significantly enriched in the mesenchymal subtype in both TCGA and CGGA datasets (Supplementary Fig. 3D). The ROC curves were used to evaluate the expression specificity of MS4A4A in the mesenchymal subtype, and the AUC was up to 92.5% in TCGA dataset, while the AUC was 91.9% in CGGA dataset (Supplementary Fig. 3E), indicating that MS4A4A may function as a potential mesenchymal biomarker of gliomas. The expression of MS4A4A might predict the survival of GBM patients in TCGA and CGGA database (Supplementary Fig. 3F, G). Single-cell sequencing was performed to verify the enrichment of MS4A4A in different cell clusters, and

we found that MS4A4A was highly expressed in macrophages, consistent with the M2 polarization markers (Fig. 2E). The IF results showed that MS4A4A had a similar location to M2 polarization marker CD163, and the expression level of MS4A4A and CD163 was associated with GBM grades (Fig. 2F). GBM organoids were a manipulatable and high-throughput model, especially for exploring the GBM microenvironment and screening drugs for GBM [30, 31]. Moreover, the GBM organoids showed consistent results that MS4A4A had co-location with M2 polarization marker (CD163) (Fig. 2G). Taken together, these results revealed that MS4A4A was associated with macrophage M2 polarization in GBM immune microenvironment.

MS4A4A regulates macrophages M2 polarization

To verify the association between MS4A4A expression and macrophage M2 polarization, we knocked down MS4A4A/Ms4a4a in THP-1 and Raw264.7 cells (Supplementary Fig. 4A–C) and subsequently polarized the macrophages with different MS4A4A expression levels to M2-phenotype by IL-4 and IL-13 treatment. According to the qRT-PCR and WB results, we chose siMS4A4A#2 THP-1 and siMS4A4A #3 Raw264.7 cells for further experiments. Compared to the control group, the siMS4A4A/siMs4a4a macrophages had significantly decreased M2 markers, such as Arg-1, TGF- β and CD206 (Fig. 3A, B and Supplementary Fig. 4D, E). The immunofluorescence assays showed that the expression level of Arg-1 was decreased in THP-1 and Raw264.7, knocking down MS4A4A/Ms4a4a (Fig. 3C, D). Moreover, we performed flow cytometry analysis and found that knocking down MS4A4A/Ms4a4a could inhibit the cell count of positive Arg-1 in macrophages (Fig. 3E, F). In addition, we established MS4A4A/Ms4a4a overexpressing THP-1 and Raw264.7 cells by the lentivirus system and proved MS4A4A/Ms4a4a expression via qRT-PCR and western blot assays (Supplementary Fig. 5A, B). The overexpression of MS4A4A/Ms4a4a in THP-1 and Raw264.7 cells elevated the M2 markers Arg-1, TGF- β and CD206 in mRNA and protein levels (Supplementary Fig. 5C–E). The IF and FACS assay results illustrated that MS4A4A/Ms4a4a overexpression could increase the Arg-1 expression and Arg-1 positive cell rate in THP-1 and Raw264.7 cells (Supplementary Fig. 5F–I), suggesting that MS4A4A plays a key role in M2 polarization in macrophages.

MS4A4A promotes macrophages M2 polarization via NF- κ B/STAT6 axis

To investigate the molecular mechanism by which MS4A4A regulates macrophage M2 polarization, we performed KEGG analysis and observed that MS4A4A was significantly positive correlated with the NF- κ B and JAK-STAT signaling pathways (Supplementary Fig. 6A). In addition, we investigated the association between MS4A4A and the polarization markers of macrophages in glioma. Based on the TCGA and CGGA datasets, we found that the M2 markers (CD163 and CD204) were positively correlated with MS4A4A expression (Fig. 4A, B). On the contrary, the M1 polarization markers of macrophage NOS2 had no significant positively correlated with MS4A4A expression in GBM (Supplementary Fig. 6B). Therefore, we speculated that MS4A4A regulated the macrophages M2 polarization via NF- κ B and JAK-STAT signaling pathways. To test the above hypothesis and mimic the effect of tumor cells on macrophages, we collected the conditional medium derived from GBM cells and treated macrophages with different MS4A4A expression levels. MS4A4A /Ms4a4a knocking down could decrease the phosphorylation of AKT, STAT6, I κ B and P65 in THP-1 and Raw264.7 cells (Fig. 4C–F). Then, we found that the overexpression of MS4A4A/Ms4a4a in macrophages could elevate the p-AKT, p-STAT6, p-I κ B and p-P65 expression level (Supplementary Fig. 6C, D). Furthermore, we detected the minimum inhibitory dose of the NF- κ B inhibitor (BAY 11-7082) and the STAT6 inhibitor (AS1517499) on THP-1 and Raw264.7 cell lines for further experiments (Supplementary Fig. 6E,

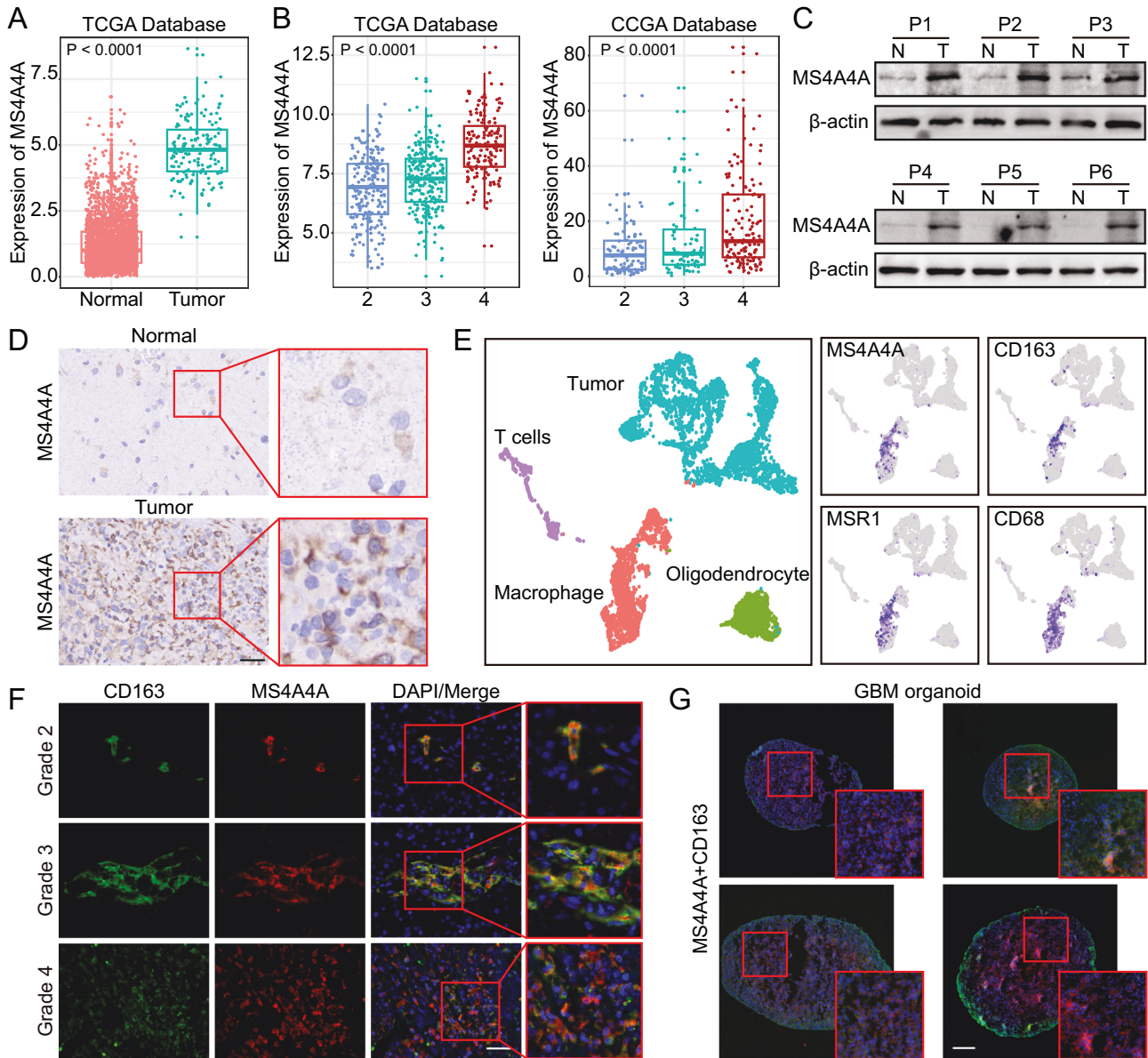


Fig. 2 MS4A4A has a relationship with poor prognosis and macrophage M2 polarization in GBM. **A** The expression of MS4A4A was significantly higher in GBM (TCGA) than normal tissues (GTEX). **B** MS4A4A was significantly increased in higher-grade gliomas in the CGGA and TCGA databases. **C** WB analysis indicated the increase of MS4A4A in normal and GBM tissues, N, normal; T, Tumor. **D** IHC assays indicated the increase of MS4A4A in normal and GBM tissues, scale bar = 50 μ m. **E** The subgroups of cells in GBM patients, MS4A4A and M2 polarization markers in macrophage group. **F** IF analysis of MS4A4A and CD163 in different grades of gliomas, scale bar = 50 μ m. **G** IF analysis of MS4A4A and CD163 (green) in GBM organoids, scale bar = 200 μ m. P values were determined by Student t test or one-way ANOVA followed by Scheffe's post hoc test.

F). We found that the inhibition of NF- κ B and JAK-STAT signaling pathways restrained the effect of MS4A4A in upregulating M2 polarization markers in macrophages (Fig. 4G, H). Taken together, these results illustrated that MS4A4A regulated macrophages M2 polarization through NF- κ B and JAK-STAT signaling pathways.

M2 macrophages mediated by MS4A4A accelerate the malignant behavior and TMZ resistance of GBM cells

The formation of immunosuppressive GBM microenvironment induced by M2 macrophages regulates the malignant biological progression and TMZ resistance [32, 33]. Based on the previous studies, we collected the conditional medium (CM) derived from PMA combined IL-4/IL-13 treated macrophages with different MS4A4A expression level and subsequently treated LN229/GL261 cells to mimic the effect of TAMs in TME on GBM cells

(Fig. 5A). Compared to the control group, MS4A4A/Ms4a4a knocking down M2 macrophages treated GBM cells had decreased proliferation capability (Fig. 5B). Additionally, the results of Transwell and cell scratch assays showed that low MS4A4A/Ms4a4a expressing M2 macrophages partly depressed the migration capability of GBM cells (Fig. 5C–E). Then, the rates of apoptotic cells in MS4A4A/Ms4a4a knockdown CM group were increased compared with those in the control group under TMZ treatment (Fig. 5F, G). Similarly, comet assays illustrated that MS4A4A/Ms4a4a knocking down macrophages caused more TMZ-induced DNA damage than the control group (Fig. 5H, I). To verify what secretory factors are regulated by different MS4A4A-expressing macrophage CM, we performed a protein chip and found that IL-10 significantly decreased in the CM of macrophages knocking down MS4A4A (Supplementary Fig. 7A, B). ELISA assays

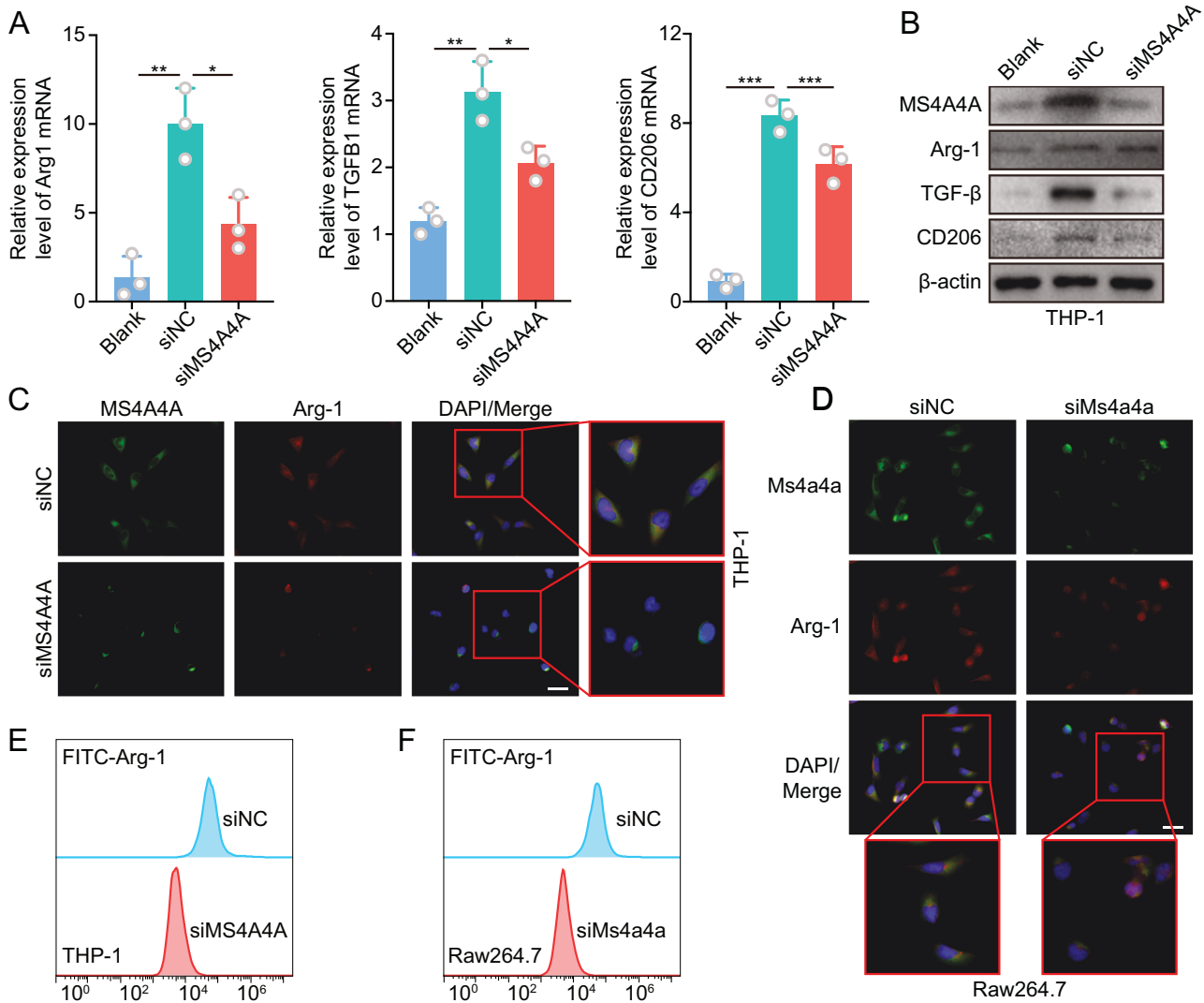


Fig. 3 MS4A4A regulates macrophage M2 polarization. **A** qRT-PCR analysis validated the indicated mRNA expression in THP-1 cells knocking down MS4A4A or the negative/blank control cells ($n = 3$). **B** WB analysis of the indicated proteins in THP-1 cells knocking down MS4A4A or the negative/blank control cells. **C** IF analysis of Arg-1 and MS4A4A in THP-1 cells, knocking down MS4A4A or the negative control cells. **D** IF analysis of Arg-1 and MS4a4a in Raw264.7 cells, knocking down MS4a4a or the negative control cells, scale bar = 20 μm. **E, F** Flow cytometry analysis of the Arg-1 positive THP-1 and Raw264.7 cells knocking down MS4A4A/Ms4a4a or the negative control cells. Data, mean \pm SD. P values were determined by Student t test. Significant results are presented as *, $P < 0.05$ **, $P < 0.01$ or ***, $P < 0.001$.

revealed that macrophages knocking down MS4A4A had lower IL-10 secretion levels (Supplementary Fig. 7C, D). The previous study revealed that IL-10 was essential for GBM cell proliferation [34] and could suppress T cell activity [35], promoting GBM progression.

Our above results revealed that the M2 polarization mediated by MS4A4A had an association with the activation of NF- κ B/STAT6 signaling. To further verify that the inhibition of NF- κ B/STAT6 signaling pathway in macrophages could improve the proliferation, migration and TMZ resistance in GBM cells, macrophages overexpressing MS4A4A/Ms4a4a were first treated with Bay 11-7082 and AS1517499. We collected CM derived from different macrophages and treated GBM cells, found that MS4A4A/Ms4a4a overexpression M2 macrophages elevated the proliferation and invasion capability in GBM cells. Conversely, the administration of NF- κ B combined with STAT6 signaling pathway inhibitors could decrease the increasing proliferation and migration capability mediated by MS4A4A/Ms4a4a overexpressing M2 macrophages in GBM cells (Supplementary Fig. 8A–F). The results of FSCS and comet assays showed that MS4A4A/Ms4a4a overexpressing M2 macrophages could reduce the apoptotic rate of

GBM cells and the DNA damage induced by TMZ. However, the inhibitor of NF- κ B/STAT6 signaling pathway in M2 macrophages enhanced the apoptosis and DNA damage in GBM cells mediated by MS4A4A/Ms4a4a overexpressing M2 macrophages under TMZ treatment (Supplementary Fig. 9A–D). Overall, these results demonstrated that the M2 polarization induced by MS4A4A/ NF- κ B/STAT6 axis dysregulation in macrophages could accelerate the malignant behavior and TMZ resistance of GBM cells.

The inhibition of the MS4A4A/ NF- κ B/STAT6 pathway enhances TMZ sensitivity and prolongs survival time in vivo

To verify the effect of the MS4A4A/NF- κ B/STAT6 pathway-induced immune-suppressive GBM microenvironment regulating TMZ resistance in vivo, we established an orthotopic mouse model of GBM by GL261 cells combined with Raw264.7 cells overexpressing Ms4a4a or the scramble cells and treated the mice with TMZ and/or BAY 11-7082 and AS1517499 (Fig. 6A). The bioluminescence imaging results illustrated that GBM derived from GL261 cells combined with Raw264.7 cells overexpressing Ms4a4a exhibited increased tumor growth and decreased mice survival compared to

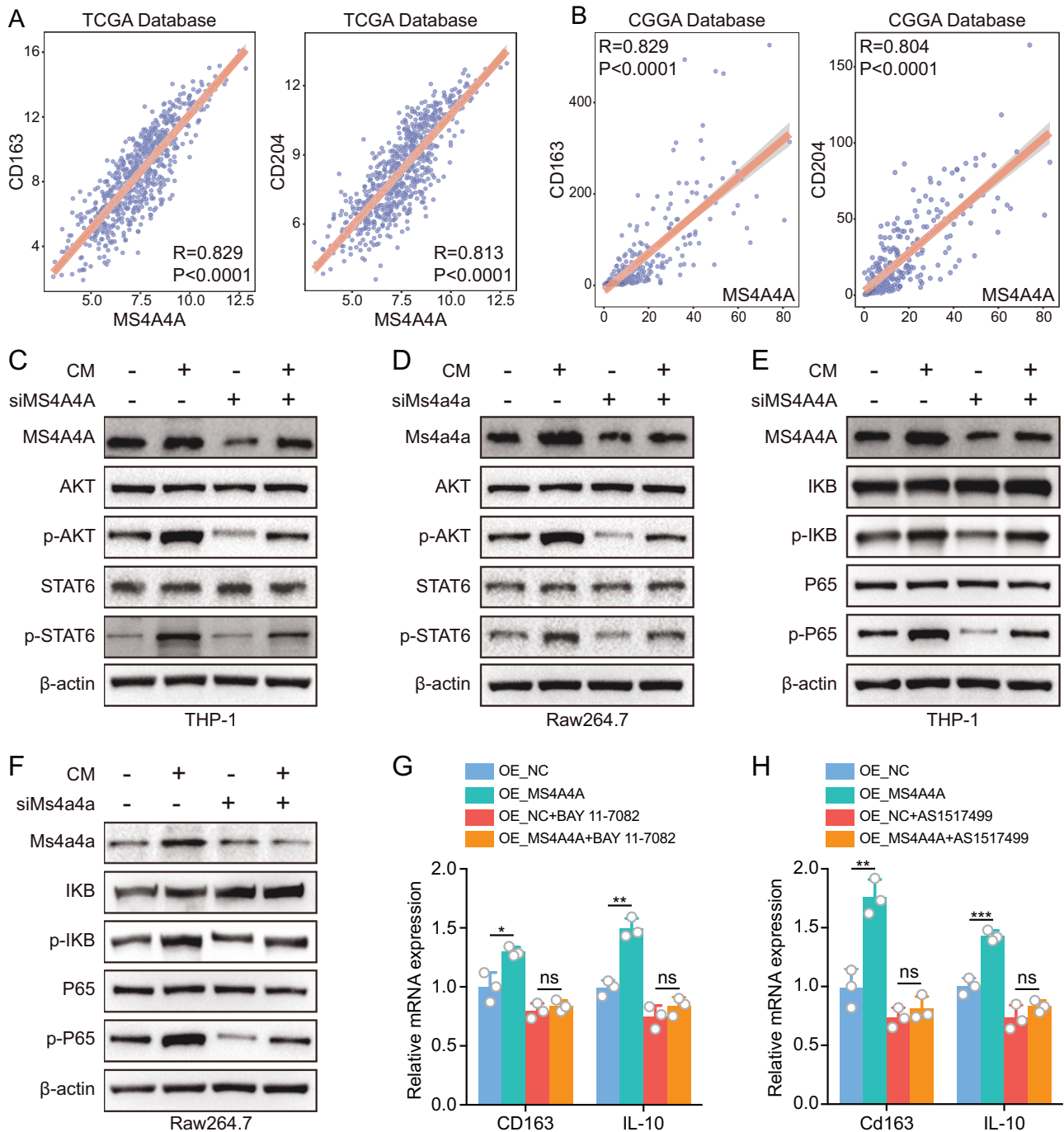
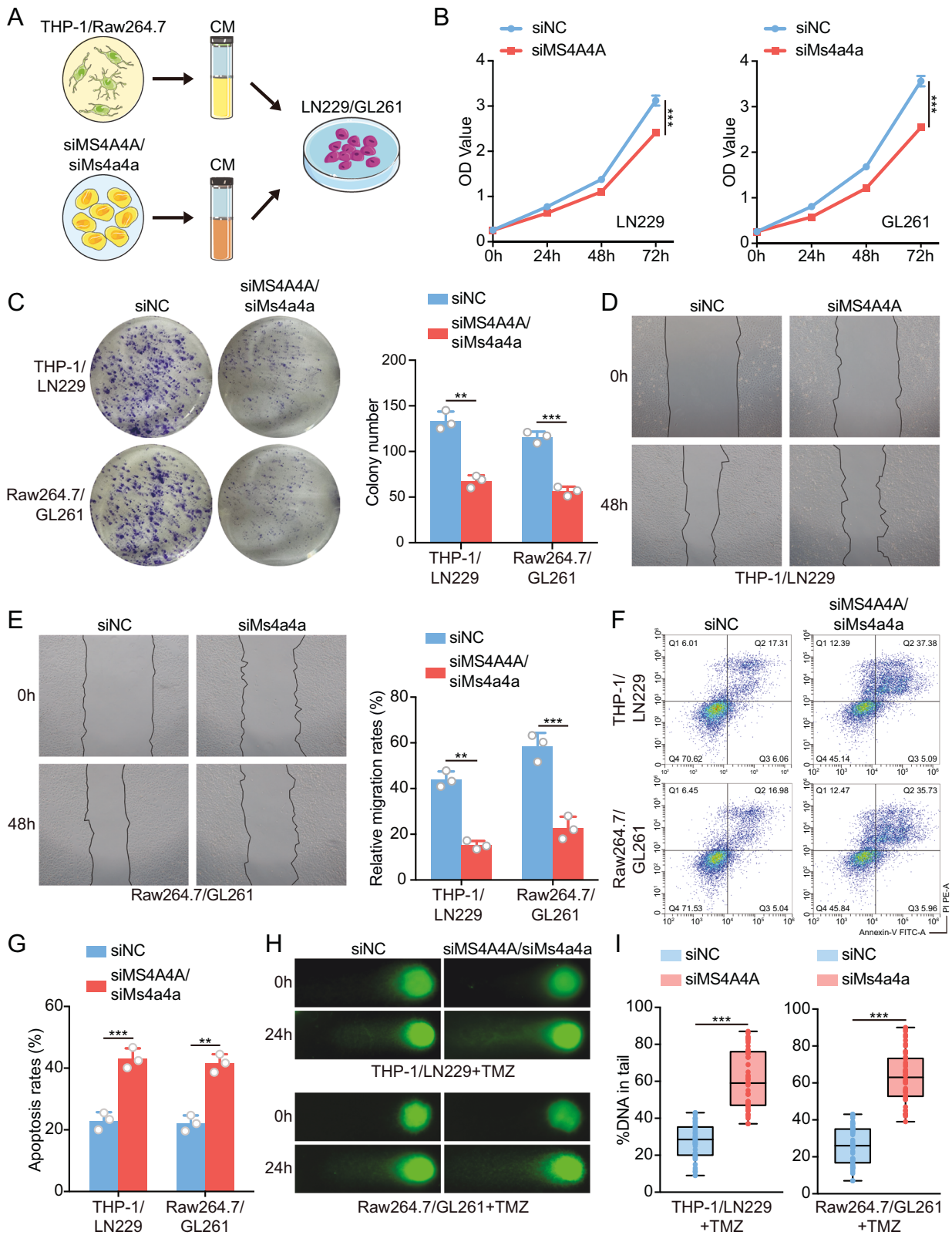


Fig. 4 MS4A4A/NF- κ B/STAT6 axis regulates macrophages M2 polarization. **A, B** The correlation analysis of CD163, CD204 and MS4A4A in TCGA database and CGGA database. **C, D** WB analysis of the indicated proteins in THP-1 and Raw264.7 cells, knocking down MS4A4A/Ms4a4a or the control cells under the treatment of CM derived from GBM cells. **E, F** WB analysis of the indicated proteins in THP-1 and Raw264.7 cells, knocking down MS4A4A/Ms4a4a or the control cells under the treatment of CM derived from GBM cells. **G, H** qRT-PCR analysis validated the indicated mRNA expression in THP-1 and Raw264.7 cells overexpressing MS4A4A or the negative control cells ($n = 3$). Data, mean \pm SD. P values were determined by Student t test. Significant results are presented as *, $P < 0.05$ **, $P < 0.01$ or ***, $P < 0.001$.

the OE_ctrl group. Moreover, the OE_Ms4a4a group mice had limited TMZ treatment response, but the inhibitors (BAY 11-7082 and AS1517499) significantly enhanced the inhibition of tumor growth induced by TMZ and prolonged the mice survival (Fig. 6B–D). To verify the synergistic effect of TMZ and inhibitor on GBM model without Ms4a4a overexpression, we established the orthotopic mouse model of GBM by GL261 cells combined with the control Raw264.7 cells and treated the mice with TMZ and/or BAY 11-7082 and AS1517499. The bioluminescence imaging

results showed that TMZ could inhibit the tumor growth, however, the combined treatment did not show significant improvement in tumor growth compared with the TMZ treatment alone. These results showed that the synergistic effect of the inhibitors on TMZ depended on the Ms4a4a expression of macrophages (Supplementary Fig. 10). Additionally, the H&E assays revealed that the inhibitors enhanced the TMZ response and decrease tumor growth in mice GBM model (Fig. 6E). IHC staining of xenograft samples demonstrated that Arg-1 expression was elevated in the



OE_Ms4a4a+DMSO/TMZ group compared to the OE_ctrl group accompanied by the increase with Ms4a4a expression. In addition, the inhibitors could reverse the elevation of Arg-1 induced by Ms4a4a through the NF- κ B/STAT6 axis. The combined treatment group had increased γ H2AX expression in mice bearing GBM

derived from GL261 cells combined with Raw264.7 cells over-expressing Ms4a4a compared with the TMZ treatment alone group (Fig. 6F, G and Supplementary Fig. 11A). Consistently, the combined treatment could significantly decrease the expression levels of Arg-1 and increase γ H2AX expression in GBM organoids

Fig. 5 M2 macrophages mediated by MS4A4A regulate malignant behavior and TMZ resistance of GBM cells. **A** The scheme of the CM derived from macrophages with different MS4A4A/Ms4a4a expression levels used to further treat GBM cells. **B** CCK-8 assays showing the proliferation of GBM cells treated with the CM from different macrophages ($n = 3$). **C** Transwell assays showing the migration of GBM cells treated with the CM from different macrophages ($n = 3$). The histogram displays the statistical results of the migration analysis. **D, E** Cell scratch assay of GBM cells treated with the CM from different macrophages ($n = 3$). The histogram displays the statistical results of the migration analysis. **F, G** Apoptosis of GBM cells treated with the CM from different macrophages under TMZ treatment. The histogram displays the statistical results of the apoptosis analysis. **H, I** Comet assay performed with GBM cells treated with the CM from different macrophages under TMZ treatment. The boxplots show the statistical results of comet assays performed with GBM cells treated with the CM from different macrophages under TMZ treatment ($n = 50$). Data, mean \pm SD. P values were determined by Student t test or two-way ANOVA followed by Tukey's multiple comparison test. Significant results are presented as **, $P < 0.01$ or ***, $P < 0.001$.

(Supplementary Fig. 11B). The safety of the combined treatment was confirmed, as no pathologic changes in the visceral organs, hematologic toxicity, and significant impacts on hepatic and renal functions were observed (Supplementary Fig. 11C; Supplementary Tables S4 and S5). Taken together, these results illustrated that the inhibition of the NF- κ B/STAT6 axis could prevent the malignant progression and TMZ resistance of GBM induced by MS4A4A-mediated macrophage M2 polarization (Fig. 7).

DISCUSSION

Glioma is a great challenge in neurosurgery in spite of the advanced therapeutic strategy, including surgery, radiotherapy, TMZ chemotherapy and immunotherapy [36, 37]. Since the remodeling of immunosuppressive GBM microenvironment, the immunotherapy efficacy is limited in GBM patients [38]. There are complex cell components of the GBM microenvironment, including endothelial cells, pericytes, fibroblasts, and immune cells [39]. TAMs are the main constituents in the TME, taking part in matrix components, immune invasion, and angiogenesis, thereby regulating tumour growth, proliferation, and chemotherapy resistance [40]. Our previous study revealed that the cross-talk between GBM cells and immune cells in glioma microenvironment, provides the theoretical evidence for the remodeling of GBM immune microenvironment and identify novel therapeutic targets [41, 42]. Nowadays, many studies have illustrated that targeting the specific immunological signature of TAMs in GBM microenvironment facilitated the rational design of immunotherapy strategies [43, 44]. Therefore, a deeper understanding of the mechanism by which GBM immune microenvironment regulating the malignant biological behavior has the potential to overcome the barrier of the diagnosis and prognosis in GBM patients.

Due to the key role of TAMs in the progression of GBM, we built a model according to the TAMs M2 polarization genes, which could predict the prognosis of GBM patients. Then, we found that MS4A4A, a M2 macrophage marker [45], had a relationship with the grade, survival time, and molecular signature of GBM. MS4A4A is selectively expressed by macrophage-lineage cells, associated with Alzheimer's disease and different types of tumors [9, 46]. However, the functions of MS4A4A in GBM and the mechanism by which MS4A4A remodeling TAMs in GBM microenvironment are still unclear. In the present study, we used GBM tissue and organoids to verify that MS4A4A were associated with the M2 macrophage markers. Herein, we established the macrophages with different MS4A4A expression levels, and observed that the overexpression of MS4A4A could promote macrophage M2 polarization. Oppositely, knockdown of MS4A4A reversed the M2 polarization of macrophages, indicating the key role of MS4A4A in regulating GBM immune microenvironment.

To further explore the mechanism of MS4A4A regulating M2 polarization in macrophages, we performed GSEA analysis and found that MS4A4A was correlated with NF- κ B and JAK-STAT6 signaling pathways. NF- κ B signaling is a pivotal pathway in mediating a variety of signaling mechanisms, biological processes, human diseases and treatment options [47]. With extensive and in-depth investigations, NF- κ B pathway is identified as a key role in development in various cancers, contributing to chemotherapy resistance, transcription factors dysregulation and microenvironment remodeling [48, 49].

Histamine secreted by glioblastoma stem cells (GSCs) could activate endothelial cells by triggering the histamine H1 receptor-Ca-NF- κ B axis, promoting angiogenesis and GBM progression [50]. Pharmacological inhibition of NF- κ B mediated immune suppression in macrophages could partly reverse the pro-tumorigenic effect induced by immunosuppressive microenvironment in breast and ovarian cancer [51, 52]. JAK-STAT signaling is an important pathway which interacts with NF- κ B, promoting the progression of cancers, inflammatory and autoimmune diseases, cardiovascular diseases, metabolic diseases, neurological diseases, and COVID-19 [47]. The inhibition of JAK-STAT signaling via shRNA or cucurbitacin-1/WP1066 administration could reduce the survival of GBM-derived brain tumor stem cells (BTSCs) regardless of endogenous MGMT promoter methylation or EGFR, PTEN, and TP53 mutational status [53]. Nowadays, the role of JAK-STAT signaling in macrophages has been widely investigated in tumor microenvironment, upregulated JAK-STAT pathway was associated with a predominant PD-1-positive and M2-like TAMs, resulting in the immune escape of tumor cells and limited immune checkpoint blockade efficacy [54, 55]. Moreover, the blocking of the JAK-STAT signaling pathway could partly rescue T-cells functionality and impair GSCs self-renewal and stemness in glioma [56, 57]. Based on the above studies and our results, we speculated that MS4A4A might regulate M2 polarization of TAMs in GBM microenvironment via NF- κ B and JAK-STAT6 signaling pathways. The macrophages with MS4A4A overexpression had a high level of p-AKT, p-STAT6, p-IKB, p-P65 and M2 markers under the treatment of GBM culture medium. In contrary, knockdown of MS4A4A could downregulate the activation of NF- κ B and JAK-STAT signaling pathways and M2 makers in macrophages. Similarly, the inhibitor of NF- κ B and JAK-STAT signaling pathways reverse the M2 polarization in macrophages, further indicating MS4A4A remodeling GBM microenvironment via NF- κ B and JAK-STAT signaling pathways.

The immunogenomics of cancers is an emerging field bridging genomics and immunology, thus, exploring the microenvironment facilitates to select appropriate tool to address various clinical questions and improve cancer patients' outcomes [58]. TAMs, as the majority of immune cells in TME, had a key effect of cancer progression via their M2 polarization, including proliferation, metastasis, and chemotherapy resistance [59]. TAMs have a relationship with the progression of GBM multiform and its development of therapeutic resistance to conventional chemotherapy [60]. In the present study, we found that MS4A4A mediated M2 polarization promoted the proliferation, invasion and TMZ resistance of GBM cells. Based on our previous study and other groups' research, many targeted GBM immune microenvironment therapy options are emerging, facilitating the development of effective personalised treatment strategies [6, 61]. In this study, we used the inhibitor of NF- κ B and JAK-STAT signaling pathways and found that the malignant biological behavior induced by MS4A4A-mediated M2 polarization could be partly reversed in GBM cells. The apoptosis and DNA damage induced by TMZ in GBM cells were increased under the administration of NF- κ B and JAK-STAT signaling pathways inhibitors. In addition, the results of the GBM xenograft mice model verified that the NF- κ B and JAK-STAT signaling pathways inhibitors elevated the survival time and decrease the tumor volume. Similar results that the inhibition of NF- κ B and JAK-STAT signaling

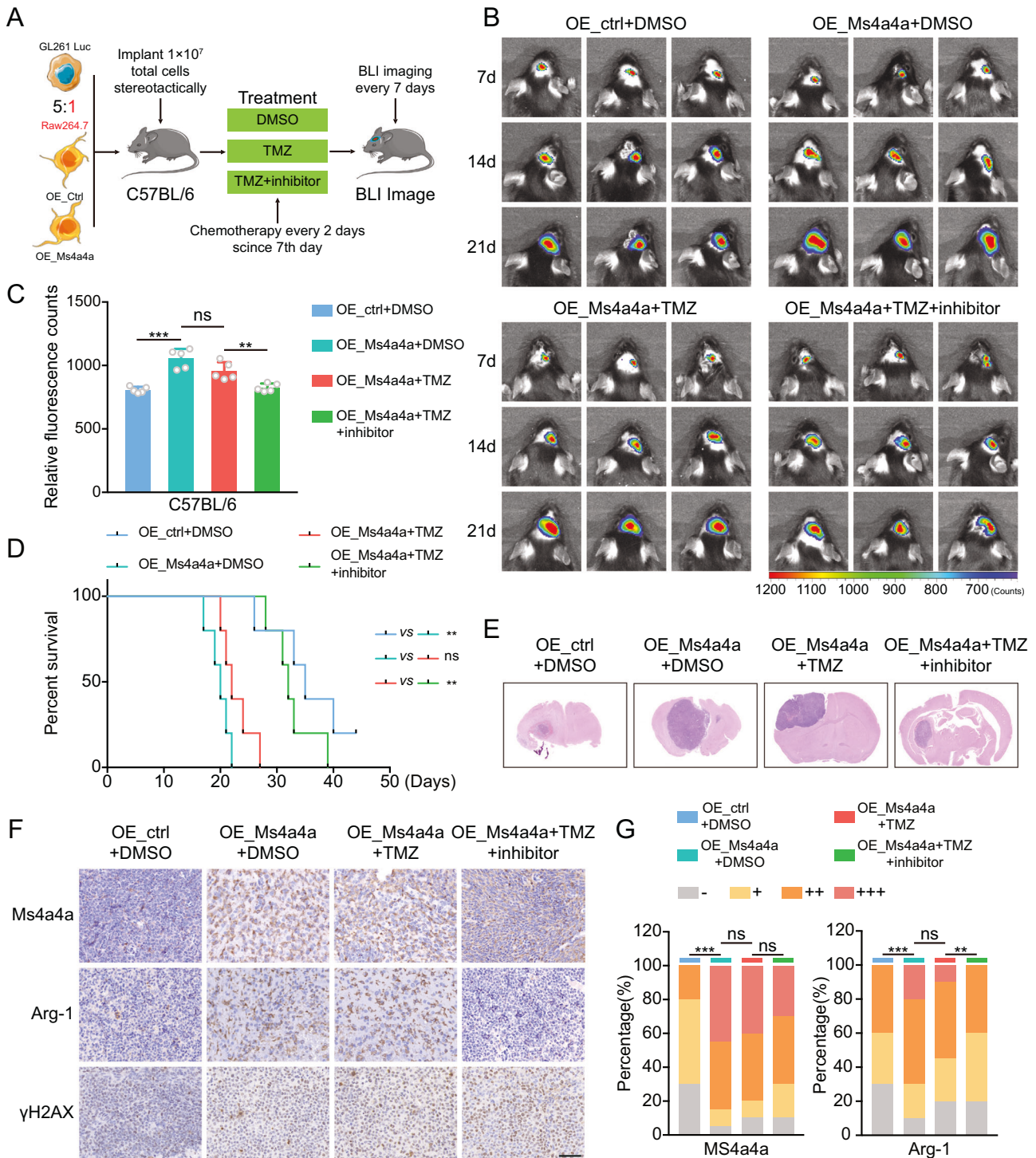


Fig. 6 Anti-MS4A4A/NF- κ B/STAT6 axis promotes chemosensitivity to TMZ in vivo. **A** Schematic diagram of establishing the orthotopic mouse model of GBM and drug administration. **B** Bioluminescence images of mice bearing tumors derived from GL261 cells combined with OE_ctrl or OE_Ms4a4a Raw264.7 cells under drug treatment at the indicated times. **C** Quantification of bioluminescence imaging signal intensities ($n = 5$). **D** Kaplan–Meier survival curves of mice bearing GBM ($n = 5$). **E** Representative H&E images of the brain isolated from mice receiving the indicated treatments. **F** The Ms4a4a, Arg-1 and CD133 levels of xenograft GBM in different groups were detected by IHC assays, scale bar = 50 μ m. **G** Quantitative evaluation of the Ms4a4a and Arg-1 expression in different group mice. Data, mean \pm SD. P values were determined by Student t test, Log-rank test or Chi-squared test. Significant results are presented as ns, nonsignificant, **, $P < 0.01$ or ***, $P < 0.001$.

pathways could attenuate the proliferation appeared in GBM organoids, suggesting that NF- κ B and JAK-STAT signaling pathways inhibitors might be a potential adjuvant agent to promote the prognosis of GBM patients.

In summary, we established that the M2-related gene LASSO model could predict the prognosis of GBM patients. And our results demonstrated that MS4A4A, an important independent prognostic factor, could regulate macrophage M2 polarization via

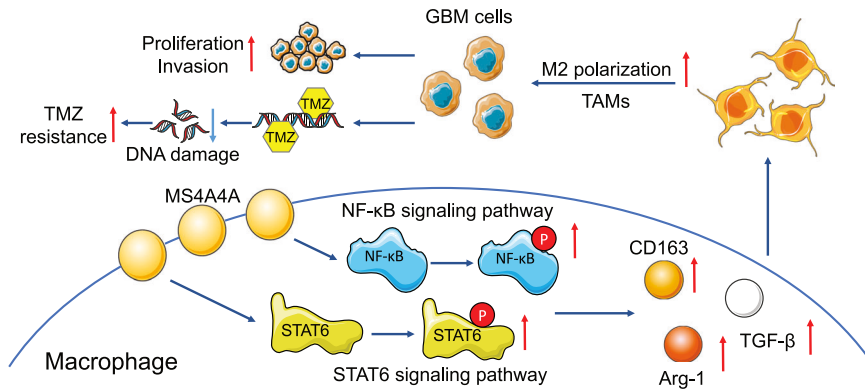


Fig. 7 The mechanistic scheme of MS4A4A regulating macrophage M2 polarization and the malignant progression of GBM cells.

the activation of NF- κ B and JAK-STAT signaling pathways in glioma microenvironment. Moreover, the formation of immunosuppressive GBM microenvironment induced by MS4A4A/ NF- κ B/ STAT axis promoted the proliferation, invasion and TMZ resistance. The inhibitor administration of NF- κ B and JAK-STAT signaling pathways could significantly attenuate MS4A4A-mediated malignant biological progression in GBM xenograft mice model and organoids. Therefore, our present work deepens the understanding of the cross-talk between microenvironment and GBM cells, suggesting that blockade of NF- κ B and JAK-STAT signaling pathways might be a novel therapeutic strategy.

DATA AVAILABILITY

All relevant data supporting the findings of this study were available in the article or from the corresponding author upon request.

REFERENCES

- Jiang T, Mao Y, Ma W, Mao Q, You Y, Yang X, et al. CGCG clinical practice guidelines for the management of adult diffuse gliomas. *Cancer Lett.* 2016;375:263–73.
- Tan AC, Ashley DM, Lopez GY, Malinzak M, Friedman HS, Khasraw M. Management of glioblastoma: state of the art and future directions. *CA Cancer J Clin.* 2020;70:299–312.
- Kirschenbaum D, Xie K, Ingelfinger F, Katzenelenbogen Y, Abadie K, Look T, et al. Time-resolved single-cell transcriptomics defines immune trajectories in glioblastoma. *Cell.* 2024;187:149–165.e123.
- Flavell RA, Sanjabi S, Wrzesinski SH, Licona-Limon P. The polarization of immune cells in the tumour environment by TGF β . *Nat Rev Immunol.* 2010;10:554–67.
- Mantovani A, Allavena P, Marchesi F, Garlanda C. Macrophages as tools and targets in cancer therapy. *Nat Rev Drug Discov.* 2022;21:799–820.
- Li Z, Meng X, Wu P, Zha C, Han B, Li L, et al. Glioblastoma cell-derived lncRNA-containing exosomes induce microglia to produce complement C5, promoting chemotherapy resistance. *Cancer Immunol Res.* 2021;9:1383–99.
- Mattiola I, Mantovani A, Locati M. The tetraspan MS4A family in homeostasis, immunity, and disease. *Trends Immunol.* 2021;42:764–81.
- Mattiola I, Tomay F, De Pizzol M, Silva-Gomes R, Savino B, Gulic T, et al. The macrophage tetraspan MS4A4A enhances dectin-1-dependent NK cell-mediated resistance to metastasis. *Nat Immunol.* 2019;20:1012–22.
- Li Y, Shen Z, Chai Z, Zhan Y, Zhang Y, Liu Z, et al. Targeting MS4A4A on tumour-associated macrophages restores CD8 $^{+}$ T-cell-mediated antitumour immunity. *Gut.* 2023;72:2307–20.
- Sun SC. The non-canonical NF- κ B pathway in immunity and inflammation. *Nat Rev Immunol.* 2017;17:545–58.
- Taniguchi K, Karin M. NF- κ B, inflammation, immunity and cancer: coming of age. *Nat Rev Immunol.* 2018;18:309–24.
- Li L, Li Z, Meng X, Wang X, Song D, Liu Y, et al. Histone lactylation-derived LINC01127 promotes the self-renewal of glioblastoma stem cells via cis-regulating the MAP4K4 to activate the JNK pathway. *Cancer Lett.* 2023;579:216467.
- Brenner D, Blaser H, Mak TW. Regulation of tumour necrosis factor signalling: live or let die. *Nat Rev Immunol.* 2015;15:362–74.
- Cheng QJ, Ohta S, Sheu KM, Spreafico R, Adelaja A, Taylor B, et al. NF- κ B dynamics determine the stimulus specificity of epigenomic reprogramming in macrophages. *Science.* 2021;372:1349–53.
- Li C, Xue VW, Wang QM, Lian GY, Huang XR, Lee TL, et al. The mincle/Syk/NF- κ B signaling circuit is essential for maintaining the protumoral activities of tumor-associated macrophages. *Cancer Immunol Res.* 2020;8:1004–17.
- Lu X, Nechushtan H, Ding F, Rosado MF, Singal R, Alizadeh AA, et al. Distinct IL-4-induced gene expression, proliferation, and intracellular signaling in germinal center B-cell-like and activated B-cell-like diffuse large-cell lymphomas. *Blood.* 2005;105:2924–32.
- Furie M. Regulation of skin barrier function via competition between AHR Axis versus IL-13/IL-4–JAK–STAT6/STAT3 axis: pathogenic and therapeutic implications in atopic dermatitis. *J Clin Med.* 2020;9:3741.
- Bi Y, Chen J, Hu F, Liu J, Li M, Zhao L. M2 macrophages as a potential target for antiatherosclerosis treatment. *Neural Plast.* 2019;2019:6724903.
- Yildiz M, Li H, Bernard D, Amin NA, Ouillette P, Jones S, et al. Activating STAT6 mutations in follicular lymphoma. *Blood.* 2015;125:668–79.
- Chi X, Tai HH. Interleukin-4 up-regulates 15-hydroxyprostaglandin dehydrogenase (15-PGDH) in human lung cancer cells. *Exp Cell Res.* 2010;316:2251–9.
- Le MK, Vuong HG, Nguyen TTT, Kondo T. NAA10 overexpression dictates distinct epigenetic, genetic, and clinicopathological characteristics in adult gliomas. *J NeuroPathol Exp Neurol.* 2023;82:650–8.
- Han X, Liu L, Huang S, Xiao W, Gao Y, Zhou W, et al. RNA m(6A) methylation modulates airway inflammation in allergic asthma via PTX3-dependent macrophage homeostasis. *Nat Commun.* 2023;14:7328.
- Wang F, Zhang S, Vuckovic I, Jeon R, Lerman A, Folmes CD, et al. Glycolytic stimulation is not a requirement for M2 macrophage differentiation. *Cell Metab.* 2018;28:463–75.e464.
- Liu X, Li Y, Qian Z, Sun Z, Xu K, Wang K, et al. A radiomic signature as a non-invasive predictor of progression-free survival in patients with lower-grade gliomas. *Neuroimage Clin.* 2018;20:1070–7.
- Wang Y, Qian T, You G, Peng X, Chen C, You Y, et al. Localizing seizure-susceptible brain regions associated with low-grade gliomas using voxel-based lesion-symptom mapping. *Neuro Oncol.* 2015;17:282–8.
- Zhao Z, Zhang KN, Wang Q, Li G, Zeng F, Zhang Y, et al. Chinese Glioma Genome Atlas (CGGA): a comprehensive resource with functional genomic data from chinese glioma patients. *Genomics Proteom Bioinforma.* 2021;19:1–12.
- Di W, Fan W, Wu F, Shi Z, Wang Z, Yu M, et al. Clinical characterization and immunosuppressive regulation of CD161 (KLRB1) in glioma through 916 samples. *Cancer Sci.* 2022;113:756–69.
- Yu K, Hu Y, Wu F, Guo Q, Qian Z, Hu W, et al. Surveying brain tumor heterogeneity by single-cell RNA-sequencing of multi-sector biopsies. *Natl Sci Rev.* 2020;7:1306–18.
- Verhaak RG, Hoadley KA, Purdom E, Wang V, Qi Y, Wilkerson MD, et al. Integrated genomic analysis identifies clinically relevant subtypes of glioblastoma characterized by abnormalities in PDGFRA, IDH1, EGFR, and NF1. *Cancer Cell.* 2010;17:98–110.
- Pawlowski KD, Duffy JT, Babak MV, Balyasnikova IV. Modeling glioblastoma complexity with organoids for personalized treatments. *Trends Mol Med.* 2023;29:282–96.
- Li G, Wang D, Zhai Y, Pan C, Zhang J, Wang C, et al. Glycometabolic reprogramming-induced XRCC1 lactylation confers therapeutic resistance in ALDH1A3-overexpressing glioblastoma. *Cell Metab.* 2024;36:1696–1710.e1610.
- Kloosterman DJ, Erhani J, Boon M, Farber M, Handgraaf SM, Ando-Kuri M, et al. Macrophage-mediated myelin recycling fuels brain cancer malignancy. *Cell.* 2024;187:5336–56.e5330.
- Zhang G, Tao X, Ji B, Gong J. Hypoxia-driven M2-polarized macrophages facilitate cancer aggressiveness and temozolomide resistance in glioblastoma. *Oxid Med Cell Longev.* 2022;2022:1614336.
- Sredni B, Weil M, Khomeinok G, Lebenthal I, Teitz S, Mardor Y, et al. Ammonium trichloro(dioxoethylene-o, o')tellurate (AS101) sensitizes tumors to chemotherapy by inhibiting the tumor interleukin 10 autocrine loop. *Cancer Res.* 2004;64:1843–52.

35. De Leo A, Ugolini A, Yu X, Scirocchi F, Scocozza D, Peixoto B, et al. Glucose-driven histone lactylation promotes the immunosuppressive activity of monocyte-derived macrophages in glioblastoma. *Immunity*. 2024;57:1105–23.e1108.
36. Ott M, Prins RM, Heimberger AB. The immune landscape of common CNS malignancies: implications for immunotherapy. *Nat Rev Clin Oncol*. 2021;18:729–44.
37. Sturm D, Pfister SM, Jones DTW. Pediatric gliomas: current concepts on diagnosis, biology, and clinical management. *J Clin Oncol*. 2017;35:2370–7.
38. Sampson JH, Gunn MD, Fecci PE, Ashley DM. Brain immunology and immunotherapy in brain tumours. *Nat Rev Cancer*. 2020;20:12–25.
39. Quail DF, Joyce JA. The microenvironmental landscape of brain tumors. *Cancer Cell*. 2017;31:326–41.
40. Chaudhuri PK, Low BC, Lim CT. Mechanobiology of tumor growth. *Chem Rev*. 2018;118:6499–515.
41. Li S, Li Z, Wang X, Zhong J, Yu D, Chen H, et al. HK3 stimulates immune cell infiltration to promote glioma deterioration. *Cancer Cell Int*. 2023;23:227.
42. Meng X, Duan C, Pang H, Chen Q, Han B, Zha C, et al. DNA damage repair alterations modulate M2 polarization of microglia to remodel the tumor microenvironment via the p53-mediated MDK expression in glioma. *EBioMedicine*. 2019;41:185–99.
43. Friebe E, Kapolou K, Unger S, Nunez NG, Utz S, Rushing EJ, et al. Single-cell mapping of human brain cancer reveals tumor-specific instruction of tissue-invasive leukocytes. *Cell*. 2020;181:1626–42.e1620.
44. Yang Y, Brown MC, Zhang G, Stevenson K, Mohme M, Kornahrens R, et al. Polio virotherapy targets the malignant glioma myeloid infiltrate with diffuse microglia activation engulfing the CNS. *Neuro-Oncol*. 2023;25:1631–43.
45. Shi ZZ, Tao H, Fan ZW, Song SJ, Bai J. Prognostic and immunological role of key genes of ferroptosis in pan-cancer. *Front Cell Dev Biol*. 2021;9:748925.
46. Naj AC, Jun G, Beecham GW, Wang LS, Vardarajan BN, Buros J, et al. Common variants at MS4A4/MS4A6E, CD2AP, CD33 and EPHA1 are associated with late-onset Alzheimer's disease. *Nat Genet*. 2011;43:436–41.
47. Guo Q, Jin Y, Chen X, Ye X, Shen X, Lin M, et al. NF-kappaB in biology and targeted therapy: new insights and translational implications. *Signal Transduct Target Ther*. 2024;9:53.
48. Bharathiraja P, Yadav P, Sajid A, Ambudkar SV, Prasad NR. Natural medicinal compounds target signal transduction pathways to overcome ABC drug efflux transporter-mediated multidrug resistance in cancer. *Drug Resist Updat*. 2023;71:101004.
49. Alsayed R, Sheikhan K, Alam MA, Buddenkotte J, Steinhoff M, Uddin S, et al. Epigenetic programming of cancer stemness by transcription factors-non-coding RNAs interactions. *Semin Cancer Biol*. 2023;92:74–83.
50. Chen J, Liu G, Wang X, Hong H, Li T, Li L, et al. Glioblastoma stem cell-specific histamine secretion drives pro-angiogenic tumor microenvironment remodeling. *Cell Stem Cell*. 2022;29:1531–46.e1537.
51. Zhang M, Liu ZZ, Aoshima K, Cai WL, Sun H, Xu T, et al. CECR2 drives breast cancer metastasis by promoting NF-kappaB signaling and macrophage-mediated immune suppression. *Sci Transl Med*. 2022;14:eabf5473.
52. Wilson AJ, Saskowski J, Barham W, Khabele D, Yull F. Microenvironmental effects limit efficacy of thymoquinone treatment in a mouse model of ovarian cancer. *Mol Cancer*. 2015;14:192.
53. Stechishin OD, Luchman HA, Ruan Y, Blough MD, Nguyen SA, Kelly JJ, et al. On-target JAK2/STAT3 inhibition slows disease progression in orthotopic xenografts of human glioblastoma brain tumor stem cells. *Neuro-Oncol*. 2013;15:198–207.
54. Han Z, Wu X, Qin H, Yuan YC, Schmolze D, Su C et al. Reprogramming of PD-1+ M2-like tumor-associated macrophages with anti-PD-L1 and lenalidomide in cutaneous T cell lymphoma. *JCI Insight*. 2023;8:e163518.
55. Minnar CM, Chariou PL, Horn LA, Hicks KC, Palena C, Schlom J, et al. Tumor-targeted interleukin-12 synergizes with entinostat to overcome PD-1/PD-L1 blockade-resistant tumors harboring MHC-I and APM deficiencies. *J Immunother Cancer*. 2022;10:e004561.
56. Ravi VM, Neidert N, Will P, Joseph K, Maier JP, Kuckelhaus J, et al. T-cell dysfunction in the glioblastoma microenvironment is mediated by myeloid cells releasing interleukin-10. *Nat Commun*. 2022;13:925.
57. Jiang L, Hao Y, Shao C, Wu Q, Prager BC, Gimple RC, et al. ADAR1-mediated RNA editing links ganglioside catabolism to glioblastoma stem cell maintenance. *J Clin Invest*. 2022;132:e143397.
58. Addala V, Newell F, Pearson JV, Redwood A, Robinson BW, Creaney J, et al. Computational immunogenomic approaches to predict response to cancer immunotherapies. *Nat Rev Clin Oncol*. 2024;21:28–46.
59. Wang Y, Zhang J, Shi H, Wang M, Yu D, Fu M, et al. M2 Tumor-Associated macrophages-derived exosomal MALAT1 promotes glycolysis and gastric cancer progression. *Adv Sci*. 2024;11:2309298.
60. Jiang S, Li W, Yang J, Zhang T, Zhang Y, Xu L, et al. Cathepsin B-responsive programmed brain-targeted delivery system for chemo-immunotherapy combination therapy of glioblastoma. *ACS Nano*. 2024;18:6445–62.
61. Yang K, Wu Z, Zhang H, Zhang N, Wu W, Wang Z, et al. Glioma targeted therapy: insight into the future of molecular approaches. *Mol Cancer*. 2022;21:39.

ACKNOWLEDGEMENTS

The authors thank Ms Hua Huang and Dr Kun Yao for tissue sample collection and clinical data retrieval.

AUTHOR CONTRIBUTIONS

WZ, ZS, TJ and ZL designed the experiments. ZC, CW, CW and ZL performed the experiments. CW, BL, CW and MY analyzed the data. ZL, YS, DW and YZ wrote the manuscript. CP, JZ, DW and YZ participated in discussions regarding this work. All the authors participated in the revision of this work.

FUNDING

This work was supported by 1. The National Natural Science Foundation of China (No. 82503572, 82072768, 82525053, 82573626); 2. Youth Beijing Scholar (No. 055); 3. The Excellent Youth Talents Program of Capital Medical University (No. A2205); 4. Foundation of Changzhou Xitaihu Institute for Frontier Technology of Cell Therapy (No. 2022-P-019); 5. Dengfeng Talents Program of Beijing Hospitals Authority; 6. Yangfan Program of Beijing Hospitals Authority (No. ZLKR202314); 7. Reform and Development Foundation of Beijing Neurosurgical Institute; 8. The Public Welfare Development and Reform Pilot Project of Beijing Medical Research Institute (No. 11000024T000003039585); 9. China Postdoctoral Science Foundation (No. 2024T170592); 10. Beijing Natural Science Foundation (JQ24057).

COMPETING INTERESTS

The authors declare no competing interests.

ETHICS APPROVAL AND CONSENT TO PARTICIPATE

The human glioma tissues were obtained from glioma patients treated in Tiantan Hospital of Capital Medical University. Informed consent was obtained from patients enrolled in this study, and the Clinical Research Ethics Committee of Tiantan Hospital of Capital Medical University approved the study protocol (KY2024-174-02). In this study, fresh GBM tissues were collected from 12 patients by surgical resection from 2023 to 2024. The inclusion criteria were as follows: patients treated by surgical resection and pathologic sampling; patients who were willing to provide disease-related materials, including pathologic diagnosis, relevant document records, medical records, and discarded GBM tissues from surgical resection; patients who were willing to provide contact information and maintain follow-up; patients who were willing to write informed consent of patients and/or the legal guardians; the researcher believed that participating in this study would not affect the treatment effect. Patients who did not meet any of the above criteria were excluded from this study. C57BL/6 mice were purchased from Beijing Vitalstar Biotechnology Co., Ltd., and bred under special pathogen-free (SPF) conditions. The Institutional Committee on Animal Care of Tiantan Hospital of Capital Medical University approved the protocols of this study (Yu2025117). All methods were performed in accordance with the relevant guidelines and regulations.

ADDITIONAL INFORMATION

Supplementary information The online version contains supplementary material available at <https://doi.org/10.1038/s41388-026-03773-1>.

Correspondence and requests for materials should be addressed to Zhongfang Shi, Tao Jiang or Wei Zhang.

Reprints and permission information is available at <http://www.nature.com/reprints>

Publisher's note Springer Nature remains neutral with regard to jurisdictional claims in published maps and institutional affiliations.



Open Access This article is licensed under a Creative Commons Attribution-NonCommercial-NoDerivatives 4.0 International License, which permits any non-commercial use, sharing, distribution and reproduction in any medium or format, as long as you give appropriate credit to the original author(s) and the source, provide a link to the Creative Commons licence, and indicate if you modified the licensed material. You do not have permission under this licence to share adapted material derived from this article or parts of it. The images or other third party material in this article are included in the article's Creative Commons licence, unless indicated otherwise in a credit line to the material. If material is not included in the article's Creative Commons licence and your intended use is not permitted by statutory regulation or exceeds the permitted use, you will need to obtain permission directly from the copyright holder. To view a copy of this licence, visit <http://creativecommons.org/licenses/by-nc-nd/4.0/>.

© The Author(s) 2026